

Article

Experimental Investigation and Numerical CFD Assessment of a Thermodynamic Breakup Model for Superheated Sprays with Injection Pressure up to 700 Bar

Francesco Duronio ^{1,*}, Angelo De Vita ^{1,2}, Alessandro Montanaro ² and Luigi Allocca ²

¹ Industrial Engineering, Information and Economics Department, Università degli Studi dell'Aquila, Piazzale Ernesto Pontieri, Monteluco di Roio, 67100 L'Aquila, Italy; angelo.devita@univaq.it

² Consiglio Nazionale delle Ricerche, Istituto di Scienze e Tecnologie per l'Energia e la Mobilità Sostenibili (STEMS), Via G. Marconi 4, 80125 Napoli, Italy; alessandro.montanaro@stems.cnr.it (A.M.); luigi.allocca@stems.cnr.it (L.A.)

* Correspondence: francesco.duronio@univaq.it; Tel.: +39-0862434317

Abstract: Among the most relevant fields of research recently investigated for improving the performance of gasoline direct injection (GDI) engines, there are ultrahigh injection pressures and the flash-boiling phenomenon. Both perform relevant roles in improving the air/fuel mixing process, reducing tailpipe emissions and implementing new combustion methods. When a high-temperature fuel is released into an environment with a pressure lower than the fuel's saturation pressure, flash boiling occurs. Due to complex two-phase flow dynamics and quick droplet vaporization, flash boiling can significantly modify spray formation. Specifically, if properly controlled, flash boiling produces important benefits for the fuel-air mixture formation, the combustion quality and, in general, for overall engine operation. Flash boiling was broadly investigated for classical injection pressure, but few works concern ultrahigh injection pressure. Here, the investigation of the spray produced by a multihole injector was performed using both experimental imaging techniques and CFD simulations aiming to highlight the combined impact of the injection pressure and the flash boiling occurrence on the spray morphology. The shadowgraph method was employed to observe the spray experimentally. The information gathered allows for assessing the performances of an Eulerian-Lagrangian algorithm purposely developed. Breakup and evaporation models, appropriate for flashing sprays, were implemented in a CFD (Computational Fluid Dynamics) code. The experimental results and the CFD simulations demonstrate a good agreement, demonstrating that through adoption of a flash-boiling breakup model, it is possible to reproduce non-evaporating and superheated sprays while changing few simulation parameters. Finally, the results also show the significance of injection pressure in preventing spray collapse.

Keywords: high-pressure; flash-boiling; converge; spray-collapse; CFD; breakup-modeling



Citation: Duronio, F.; De Vita, A.; Montanaro, A.; Allocca L. Experimental Investigation and Numerical CFD Assessment of a Thermodynamic Breakup Model for Superheated Sprays with Injection Pressure up to 700 Bar. *Fluids* **2023**, *8*, 155. <https://doi.org/10.3390/fluids8050155>

Academic Editor: D. Andrew S. Rees

Received: 8 April 2023

Revised: 26 April 2023

Accepted: 10 May 2023

Published: 14 May 2023



Copyright: © 2023 by the authors. Licensee MDPI, Basel, Switzerland. This article is an open access article distributed under the terms and conditions of the Creative Commons Attribution (CC BY) license (<https://creativecommons.org/licenses/by/4.0/>).

1. Introduction

One of the most promising approaches to reduce the environmental impact of the light-duty transportation sector is generally acknowledged to be the employment of direct-injection spark-ignition propulsion systems gasoline-fueled (GDI), which enable engine downsizing and the use of improved combustion techniques [1,2]. However, further improvements are required to boost GDI engines performance and limit, among the other, the liquid film formation that triggers soot production [3]. The injection process plays a significant role in GDI engines and significantly impacts the chain of events that leads to mixture formation, combustion and pollution creation. Direct injection techniques into the cylinder require that the liquid fuel is broken up into tiny droplets and quickly evaporated in order to ensure an effective mixture formation [4–6].

It was shown that both high injection pressure as well as flash boiling improve spray characteristics [7]. According to previous scientific studies, fuel injection at high pressure levels (up to 1500 bar) enhances both fuel evaporation and in-cylinder turbulence giving, at the end, a more stable combustion [8]. The injection pressure affects the breakup dynamics and droplet dimensions, as shown by Yamaguchi in an in-depth investigation on spray evolution [9]. In another work, spray penetration and breakup time of high-pressure sprays were related to literature correlations for diesel injections [10]. On the other hand, liquid atomization by flash boiling mechanism is another potential method for achieving high-quality spray with a small and narrow drop-size distribution [3,11–16].

When the liquid fuel at high pressure and temperature (near its boiling point) is discharged through an orifice to a low ambient pressure (which is below its saturation pressure), flash boiling sprays are generated. The compressed liquid is expanded below its saturation pressure; vapor bubbles arise, and their continued expansion will produce severe spray atomization.

However, when flashing sprays are issued from multihole injectors, the single plumes deviate toward one another and combine into a single jet. This phenomenon is the so-called “spray collapse” and frequently takes place in flashing sprays. A collapsed spray causes spray-wall impingement (which increases the generation of exhaust soot) and it greatly reduces the combustion quality [7,17,18].

Flash boiling onset and injection pressure are intimately coupled. High injection pressure does more than just produce sprays with small drop sizes; it also prevents spray collapse and facilitates the vaporization of liquid fuel [19,20]. Therefore, it seems inevitable to develop a detailed understanding of the flash boiling injections, exploiting both experimental and numerical methods—in particular, when extremely high injection pressures are adopted. Eulerian–Lagrangian spray simulations are a smart and efficient tool for simulating the evolution of liquid sprays with limited calculation times that are in line with industry standards and that fit with the integration of such spray models in whole engine simulations. The breakup model is an important component of this approach. Conventional approaches, such as Kelvin–Helmholtz–Rayleigh–Taylor (KH–RT) and Reitz–Diwakar (RD), are based on the idea that liquid droplet breakage is caused by superficial aerodynamic instabilities and is primarily dependent on the relative velocity between liquid and gas phases. However, when a superheated liquid is injected, the vapor bubbles that form inside the liquid core also contribute to the breakup. Therefore, without adjusting certain constants, aerodynamic breakup techniques alone cannot replicate the various flash-boiling situations and, in particular, provide unrealistic droplet sizes [21,22]. An effervescent breakup model developed expressly to account for bubble expansion within droplets in flash-boiling sprays exhibited significant improvement for Lagrangian spray simulations [23] and so is strongly advised. It is a distinct primary breakup mechanism that interacts with the aerodynamic breakup and considers droplet shattering as a result of thermodynamic nonequilibrium conditions.

So, this paper focuses on the investigation of high-pressure liquid sprays in both non-evaporative and flash boiling conditions performed with experimental and numerical methods. The spray morphology was investigated under various thermodynamic conditions, and, in particular, the performance of the developed effervescent breakup model in simulating the behavior of high-pressure spray under flash boiling conditions was assessed. Common GDI injectors operate with a rail pressure of roughly 200 bar while current contribution deals with values up to 700 bar. The discussed CFD methodology was validated using the experimental images obtained using nonintrusive techniques. The outcomes of the research highlight that the adoption of the effervescent breakup model for flashing spray improves the result’s quality and avoid further tuning of the breakup parameters. The work is organized into three sections: Research Methodology, Discussion of the Result and Conclusions. The Research Methodology is structured into two subsections. The first one illustrates the experimental measurement performed; next, the CFD code and the effervescent breakup model are presented. Results are organized into three subparagraphs. Initially, the modeling

approach adopted was assessed comparing the numerical results with the experiments. Next, details concerning the effervescent breakup model are discussed. Last, deepening about the spray morphology and the role played by flash boiling onset are presented.

2. Research Methodology

A stepped-hole valve-covered orifice (SVCO) injector with 10 holes and 90° outer cone angle was considered in this study. Table 1 lists the key characteristics of the device.

Table 1. Principal features of the GDI injector.

Spray shape	Circular
Nozzle type	VCO (Valve-covered orifice)
Nozzle shape	Stepped-hole
Orifice length	700 μm
Orifice diameter	100 μm
L/D ratio	7
Orifice drill angle	35.5°/45°
Full outer angle	90°
Flow rate	10.55 cc/s @ 100 bar
Discharge Coefficient	0.737 @ 400 bar/0.937 @ 700 bar

The conditions investigated are summarized in Table 2.

Table 2. Investigated operating conditions.

	Case HP	Case HP-fb	Case vHP	Case vHP-fb
Injection Pressure [bar]	400	400	700	700
Fuel Temp. [K]	293	363	293	363
Ambient Pressure [bar]	1	0.2	1	0.2
Ambient Temp. [K]	293	293	293	293

Cases HP (high-pressure) and vHP (very high-pressure) examine nonevaporative gasoline sprays, while cases HP-fb and vHP-fb refer to intense evaporation conditions or, more easily, flash boiling. The fuel temperature is increased to 363 K and ambient pressure is lowered to 0.2 bar. Nitrogen inert gas was used to fill the combustion vessel and realize the desired back-pressures. CFD simulations were validated comparing spray penetration length and shape exploiting experimental images acquired using the shadowgraph optical technique. The flash-boiling breakup model developed by the authors for the CFD simulations was implemented in CONVERGE 3.0 as a User Defined Function (UDF).

2.1. Experimental Equipment and Setup

The spray evolution was investigated using Z-type shadowgraph imaging technique, based on the variations of the refractive index. The light source is a pulsed LED (Omicron LEDMOD V2—470 nm/450 mW). Figure 1 presents a scheme of the optical setup: two off-axis parabolic mirrors ($f = 508$ mm, $d = 101.6$ mm) are mounted in front of the optical windows of the chamber.

High-intensity flash was used as light source. An high-speed C-Mos camera (Photron FASTCAM SA4) equipped with a 90 mm optics lens was used to acquire spray images. The camera was synchronized with both the injection system and the LED. The imaging was performed at a shutter speed of 16.000 frames per second (fps) with an image dimension of 512 per 448 pixels. The exposure time of the high-speed camera was set to 3.26 μs , while a spatial resolution of 5.9 pixel/mm was obtained by the described setup. The spray images

were processed by ad-hoc developed postprocessing procedure [20,24] allowed to identify the contours of the jet in the nitrogen gas and measure the main parameters characterizing the spray structure. The investigations were performed on an optically accessible constant-volume vessel where the thermodynamic conditions of a combustion chamber, at injection time, were reproduced. Full details of the experimental apparatus are reported in [25,26] and hereafter, only a brief description is provided. Fuel injection mainly includes a fuel supply system, which is used to supply fuel from a fuel storage container to the injector. The pressurized fuel was conveyed inside the common rail, where an electronic pressure regulator and a pressure transducer mounted on the rail allowed the setting and reading of the pressure value, respectively, set through a homemade electronic control unit (ECU). The injector was fixed at the top of the CVC in a specific holder, featuring a jacket for the temperature control of the nozzle nose, connected to a chiller for cooling liquid circulation. The fuel was heated by electrical resistance and controlled in temperature by a J-type thermocouple. Nozzle and fuel temperature management was performed with a governor via remote computer. A customized injector equipped with a thin thermocouple was used to calibrate liquid temperature for the jacket and the nozzle nose. Both injector and fuel temperature were kept constant at 293 K for cases HP and vHP while they were increased at 363 K for flashing conditions (Table 2). The injector and the acquisition system were activated in a synchronous mode with an external TTL signal that previously starts the ECU. The acquisitions were repeated five times to take into account for cycle-to-cycle variations.

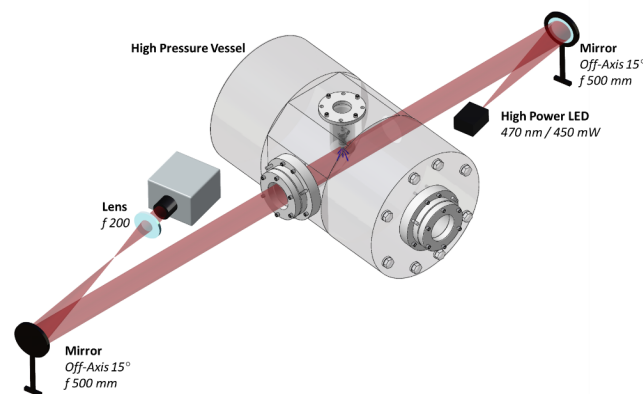


Figure 1. Scheme of the experimental apparatus highlighting the optical shadowgraph configuration.

2.2. Computational Method

The simulations were carried out with an Eulerian–Lagrangian approach. A modified PISO algorithm was adopted for the solution of the governing equations of the continuum-phase [27]. The idea behind the present contribution is to use a fixed parameter setup to simulate both nonevaporative and flash-boiling conditions. For this purpose, the developed effervescent breakup model is activated only in flash-boiling conditions to account for the thermodynamic breakup mechanism together with an improved vaporization model. Therefore, it is appropriate to provide a detailed description of the phase change, heat transfer and flash-boiling breakup models essential for simulating flash-boiling conditions. Among other effects, the nucleation of vapor bubbles within the liquid droplets triggers a thermodynamic breakup mechanism that is approximately ten times faster in comparison with the classical aerodynamic breakup [28,29]. Based on this consideration, an effervescent thermodynamic breakup model, named **fbBreakup**, was developed as an UDF within CONVERGE CFD code [30]. The secondary aerodynamic breakup was modelled with the Reitz–Diwakar model [31,32].

Figure 2 shows the effervescent breakup of the bubble–droplet system.

The liquid is injected in superheated conditions and so vapor bubbles nucleate within the liquid ligaments [31]. Their initial radius, $R_{i,0}$, is described by Equation (1) and represents a dynamic equilibrium between the pressure forces and the liquid surface tension (σ):

$$R_{i,0} = \frac{2\sigma}{P_{sat}(T_0) - P_\infty} \tag{1}$$

where P_∞ is the ambient pressure computed in the Eulerian framework and P_{sat} is the liquid saturation pressure. T_0 is the liquid droplet temperature. If the vapor bubbles have a radius smaller than this value, they collapse under the force of the surface tension. $R_{i,0}$ is called the critical radius because any variation of the pressure difference “ $P_{sat}(T_0) - P_\infty$ ” will cause the bubble to grow or collapse. According to the Rayleigh–Plesset equation and neglecting cooling effects from evaporation and thermal diffusion to the bubble surface (inertial-dominated growth), the bubble growth rate was calculated as follows.

$$V_i = \sqrt{\frac{3}{\rho_l}(p_{sat} - p_\infty)} \tag{2}$$

This assumption can be accepted because for a bubble growing in a superheated droplet, the timescales from initiation to droplet breakup are in the order of tens of microseconds and so faster than vaporization and heat exchange phenomena [33] The droplet growth rate is related to the bubble growth rate as follows [29]:

$$V_o = V_i \cdot \Delta^2 \tag{3}$$

The breakup of the bubble + droplet system is driven by instabilities that grow along the droplet and bubble surfaces represented in Figure 2a. The instability growth rate ω is the largest real root of the following normalized growth rate equation [29]:

$$(\Delta - \Delta^2 - \psi_o \Delta)\Omega^2 + (-1 + \Delta^4 + \psi_o)We_o^{1/2}\Omega + 2\Delta^2 + 2\Delta^{-2} - 3\psi_i \frac{We_i}{Ma_i^2} \frac{\Omega}{\Omega + 3We_i^{1/2}} \Delta^2 = 0 \tag{4}$$

where:

$$\begin{aligned} \Omega &= \sqrt{\frac{\rho_l R_i^3}{\sigma}} \omega, \quad \rightarrow \quad We_o = \frac{\rho_l V_o^2 R_i}{\sigma}, \quad \rightarrow \quad We_i = \frac{\rho_l V_i^2 R_i}{\sigma} \\ Ma_i &= \frac{V_i}{c} \quad \rightarrow \\ \Delta &= \frac{R_o}{R_i}, \quad \rightarrow \quad \psi_o = \frac{\rho_{go}}{\rho_l}, \quad \rightarrow \quad \psi_i = \frac{\rho_{gi}}{\rho_l} \end{aligned} \tag{5}$$

V_i and V_o are the bubble and droplet growth rate previously discussed, while ρ_{gi} and ρ_{go} are the gas densities within and outside the bubble + droplet system. The following relationship describes the temporal evolution of this instability, denoted with η , which grows with the rate ω :

$$\ln\left(\frac{\eta}{\eta_0}\right) = \int_0^t \omega dt \tag{6}$$

When the instability amplitude becomes larger than a characteristic length of the spray (Figure 2b) [34], which can be chosen equal to the film thickness (i.e., the difference between droplet and bubble radius $R_o(t) - R_i(t)$), breakup takes place. It follows that the breakup criterion is equal to:

$$k_b(t) = \frac{\eta_0 e^{\int_0^t \omega dt}}{R_o(t) - R_i(t)} \tag{7}$$

where the initial disturbance η_0 is: $\eta_0 = 0.05 \cdot R_o(t_0)$. Breakup occurs at $t = t_b$ when the instability amplitude equals the film thickness ($k_b(t_b) = \bar{k}_b = 1$). \bar{k}_b is a model constant that acknowledges the complexities that can be found in reality. In the present investigation, it is assumed equal to the unity. The flash boiling breakup is a catastrophic breakup because it leads to an explosion of the droplet, the expansions of the plumes and thus the plume-to-plume interaction. To reproduce this behavior, once the breakup occurs, a radial velocity component is added to the original velocity of the droplet as shown in Figure 3.

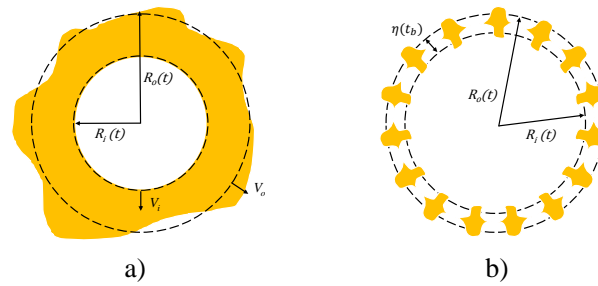


Figure 2. Time evolution of bubble–droplet system. (a) The breakup of the bubble + droplet system is driven by instabilities that grow along the droplet and bubble surfaces. (b) When the instability amplitude becomes larger than a characteristic length of the spray.

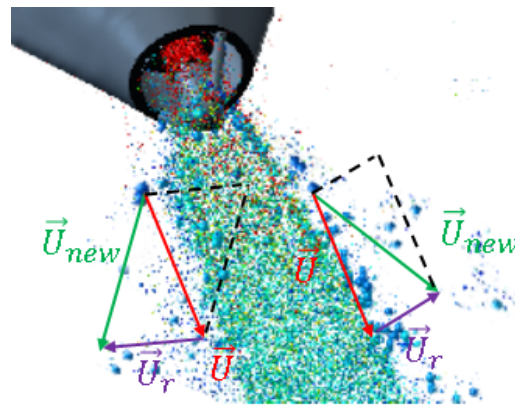


Figure 3. Droplet velocity after breakup updating.

The magnitude of the radial velocity (U_r) is obtained from mass and momentum conservation before and after breakup [29]:

$$U_r = k_v \frac{3R_i^2 V_i (R_o - R_i)}{R_o^3 - R_i^3} \tag{8}$$

It follows that the new velocity components, after breakup, are equal to:

$$U_x = U_{x,old} + U_{xr} \quad U_y = U_{y,old} + U_{yr} \quad U_z = U_{z,old} + U_{zr} \tag{9}$$

U_r vector lies on a plane perpendicular to the initial velocity vector of the parcel and it has a random orientation. k_v is a coefficient for scaling the radial velocity. Here, it is set equal to the unity. The size of droplets after breakup can be calculated with following relation obtained from the conservation of mass and energy [29].

$$SMR_{32}^{-1} = \frac{1}{2} \frac{R_o^2 + R_i^2}{R_o^3 - R_i^3} + \left(\frac{3}{2} \frac{R_i^4 (R_i^{-1} - R_o^{-1})}{R_o^3 - R_i^3} V_i^2 - \frac{U_r^2}{2} \right) \frac{\rho_l}{3\sigma} \tag{10}$$

where SMR_{32} is the Sauter Mean Radius.

Mass conservation during the breakup process is obtained updating the number of particles in each parcel:

$$n_{new} d_{new}^3 = n_{old} d_{old}^3 \tag{11}$$

where n_{old} and n_{new} are the number of particles, respectively, before and after breakup.

Each parcel can experience the flash-boiling breakup only one time. After that, it undergoes on aerodynamic breakup. Differently from the flash-boiling breakup, the latter can be applied multiple times. A specific input parameter allow to activate the fbBreakup model when flashing conditions were simulated. This combined thermodynamic–aerodynamic

breakup model was validated in previous works of the authors, but in the present contribution, it will be extended to ultrahigh injection pressure conditions [23,28].

Further than modifying the breakup mechanism, flash boiling strongly influences the phase change process. Amsden’s energy balance was used to simulate heat transfer within droplets. The Ranz–Marshall correlation is applied to determine the rate of heat transfer per unit area. Full details and complete descriptions can be found in [30,35,36].

Price models was adopted for describing superheated liquid phase transition [37]. In such a model, the evaporation rate is given by two components: the subcooled and superheated terms. The subcooled term is computed as:

$$\frac{dM_{Sc}}{dt} = 2\pi R P_{\infty} \frac{Sh D_i}{T_f R_f} \ln\left(\frac{P_{\infty} - P_v}{P_{\infty} - P_S}\right) \tag{12}$$

where:

- R : drop radius;
- P_{∞} : ambient pressure;
- Sh : nondimensional Sherwood number, function of Reynolds and Schmidt numbers:

$$Sh = 2 + 0.6Re^{0.5}Sc^{0.33} \tag{13}$$

- D_i : binary diffusivity coefficient;
- T_f : vapor film temperature (average of the temperatures of the droplet and of the surrounding gas);
- R_f : vapor film specific gas constant;
- P_v : partial vapor pressure of the liquid species;
- P_{sat} : saturation pressure.

The superheated term is:

$$\frac{dM_{sh}}{dt} = \frac{4\pi R^2 \alpha (T_d - T_b)}{H_L} \tag{14}$$

where:

- H_L : latent heat of vaporization of the liquid;
- T_b : boiling temperature of the fuel at the specific ambient pressure;
- T_d : droplet temperature;
- α : heat transfer empirical coefficient [31].

It follows that the total evaporation rate is:

$$\frac{dM_t}{dt} = \frac{dM_{Sc}}{dt} + \frac{dM_{sh}}{dt} \tag{15}$$

The other physical submodels, present in the Lagrangian simulation, are reported in Table 3.

Table 3. Lagrangian framework physical submodels.

Injection model	Flow Rate + Discharge
Effervescent Breakup	fbBreakup
Aereodynamic Breakup	Reitz–Diwakar
Heat transfer	Ranz–Marshall
Vaporization	Frossling + Flash Boiling Vaporization
Collision	No Time Counter (NTC)
Coalescence	Post and Abraham
Dispersion	O’Rourke

Figure 4 shows the mass flow rate profiles measured by the injector manufacturer.

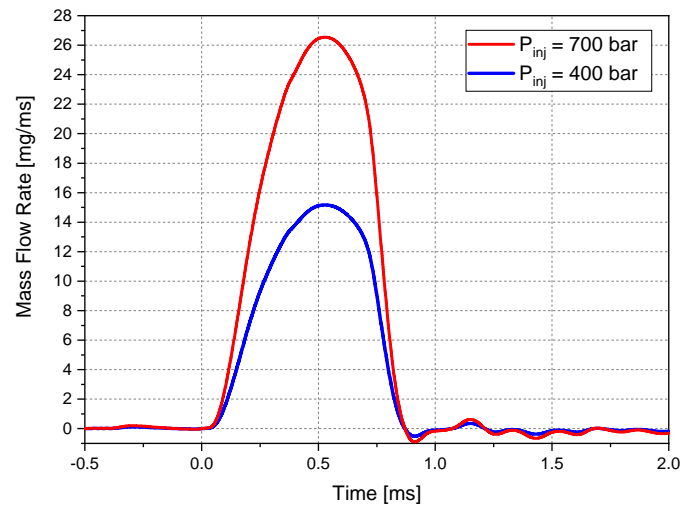


Figure 4. Mass flow-rate profiles for the two injection pressures.

The parcel count for a grid of 0.125 mm is equal 200,000 parcels per nozzle accordingly with [30,38]. Parcels were initialized with a diameter equal to the nozzle one as reported in Table 1. The cone angle of the spray was measured from experimental images and set equal to 16° and 24° for, respectively, cases HP/vHP and cases HP-fb/vHPfb. Table 4 reports the parameters for the aerodynamic breakup. The Reitz–Diwakar’s constants C_{bag} , C_b , C_{strip} and C_s are set equal for both flash boiling and ambient conditions.

Table 4. Breakup model parameters.

k_b	1
k_v	1
C_{bag}	6
C_b	1.5
C_{strip}	1
C_s	10

The injection environment is a cylinder with a height of 0.75 m and a diameter of 0.150 m, which matches the constant volume chamber used in the experiments. The domain was discretized using the internal CONVERGE mesh tool [30,39] with a 2 mm base grid, a fixed embedding refinement zone in the near nozzle area and an adaptive mesh refinement (AMR) depending on the velocity gradient for the spray development. Three different grid levels were tested: coarse, base and fine, characterized by different embedding and AMR levels. Table 5 reports all the details.

Table 5. Description of the different grids adopted for CFD simulations.

	AMR and Fixed Embedding Level	Grid Size
Coarse	2	500 μm
Base	3	250 μm
Fine	4	125 μm

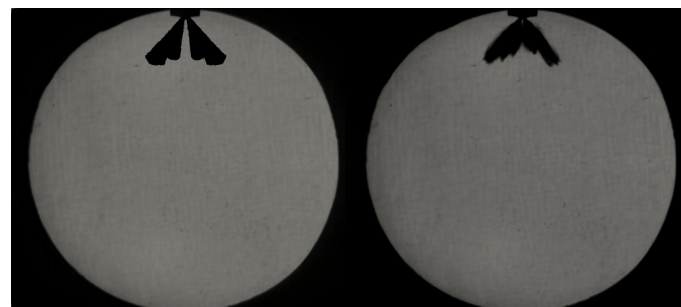
The injection environment is filled with nitrogen and RANS RNG-k-ε model used for turbulence modeling [21,32]. Numerical results were postprocessed using Paraview software.

3. Discussion of the Results

Experimental images were used to validate qualitatively and quantitatively the CFD simulations. The performances of the effervescent breakup model were assessed. Additional information not available from the shadowgraph images, such as droplet velocity and size, were also investigated to provide insights into spray structure.

3.1. Validation with Shadowgraph Acquisitions

Figure 5 reports, for case vHP, a comparison of the CFD spray shape (on the left) against the shadowgraph images (on the right) at different temporal instants after the start of injection (SOI).



(a) $t_{SOI} = 0.125$ ms



(b) $t_{SOI} = 0.375$ ms



(c) $t_{SOI} = 0.625$ ms

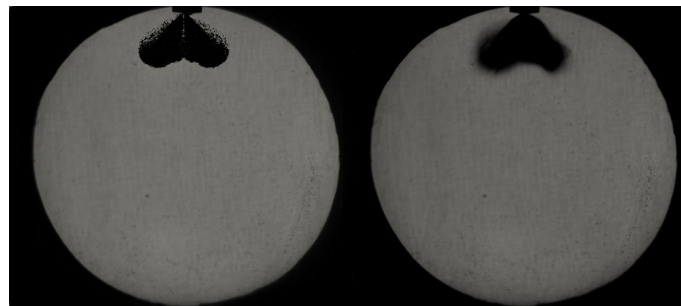
Figure 5. Comparison between numerical and experimental results for case vHP.

The CFD model properly reproduce the V-shaped plumes experimentally observed and the evolution of the spray is correctly reproduced.

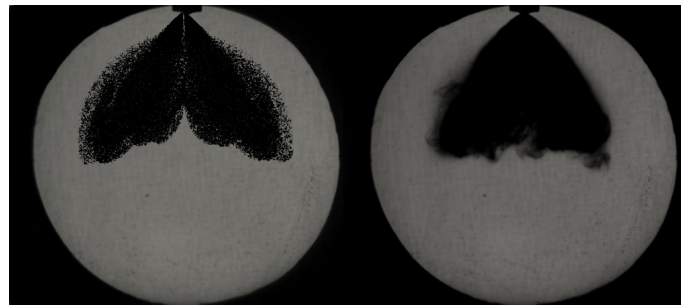
Figure 6 shows the same comparison but for the case vHP-fb.

The single plumes of the spray are clearly recognizable from the case vHP images (Figure 5), while, when the liquid is injected in superheated conditions (case vHP-fb-Figure 6), the plumes interact with each other, making it almost impossible to distinguish their profiles and appearing as a single large jet. This is an effect of the strong effervescent breakup, which promotes the interaction between the single plumes spreading liquid droplets in every direction and entailing greater compactness of the spray. It is interesting

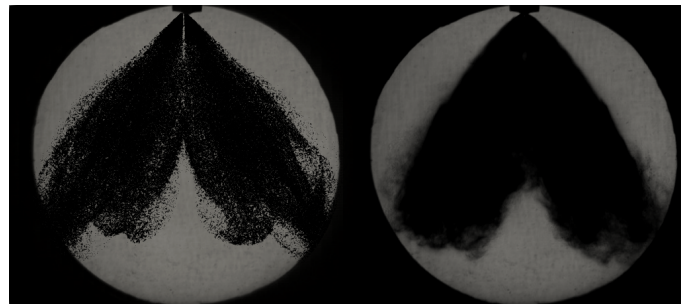
to observe that the spray collapse is almost completely avoided, despite being the superheat degree really high. This is a consequence of the high spray momentum owned by the droplet considering the 700 bar of injection pressure. As reported in Figure 7, the agreement between experiments and simulations is quite good also for the cases HP and HP-fb characterized by a lower injection pressure (equal to 400 bar). The spray shapes obtained from CFD simulations are compared against the shadowgraph images taken at 0.43 ms times after the start of injection (SOI).



(a) $t_{SOI} = 0.125$ ms



(b) $t_{SOI} = 0.375$ ms



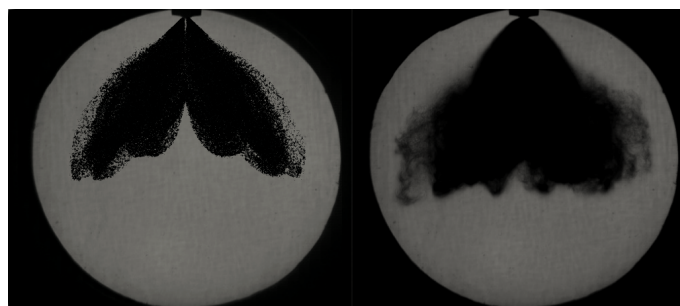
(c) $t_{SOI} = 0.625$ ms

Figure 6. Comparison between numerical and experimental results for case vHP-fb.



(a)

Figure 7. Cont.



(b)

Figure 7. CFD results and experimental shadowgraph images for cases HP (a) and vHPfb (b). $t = 0.43$ ms after the SOI.

A quantitative validation can be performed comparing the spray penetration measured from the experiments and the one computed from the simulations.

Figures 8 and 9 depicts a comparisons of experimental and numerical liquid penetration for all the simulated cases.

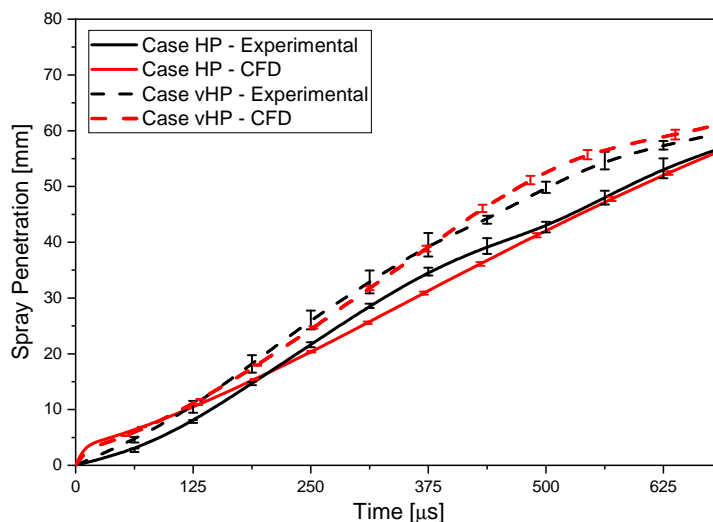


Figure 8. Numerical and experimental liquid penetration for case HP and vHP vs. time.

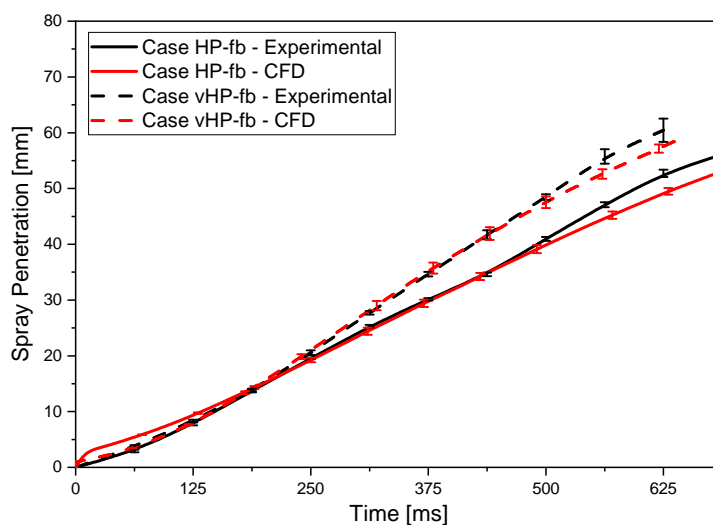


Figure 9. Numerical and experimental liquid penetration for case vHP-fb and 2fb vs. time.

The penetration length was assumed as the maximum axial distance of any plume, measured from the injector tip, in the direction of the injector axis. The numerical penetration was computed as the axial distance from the injector where 99% of the liquid mass. The experiments were repeated five times to take into account for cycle-to-cycle variations. The uncertainty bars in the graphs report the variance from the average value. The simulations performed with the three different grid levels were used to assess the uncertainty of the numerical results. The criterion illustrated by Roache in [40], where the assessment procedures adopted by the AIAA, ITTC and IEEE are described and discussed in detail, was adopted for the purpose. The penetrations measured from the experimental images and those computed from the simulations are in quite good agreement, and the differences are almost always limited within the uncertainty bars. Only few differences can be found in the initial stages of the injections. These can be related to cavitation or flash-boiling phenomena that could take place within the injector. The jets of cases vHP and vHP-fb penetrate faster if compared to the ones of cases HP and HP-fb, respectively. The higher injection pressure gives an higher momentum to the liquid droplets. It is important to underline that, with this modeling approach, the same breakup constant can be used for simulating both non-evaporative and flash-boiling conditions.

3.2. Insights about the Flash Boiling Breakup Model

This section aims to assess the benefits of using the effervescent breakup model in the simulation of superheated sprays. The droplets' size and the vaporization process were investigated. A further simulation, concerning case HP-fb, was performed adopting the **Reitz-Diwakar** model alone deactivating the **fbBreakup** model. The penetration lengths computed using **Reitz-Diwakar** and **fbBreakup+Reitz-Diwakar** breakup models are compared with the one experimentally measured in Figure 10.

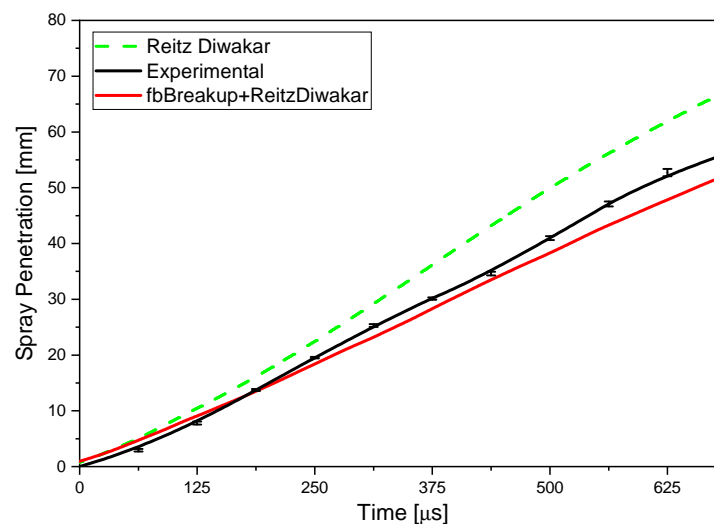


Figure 10. Comparison of the numerical penetration curves computed using Reitz–Diwakar and fbBreakup breakup models with experimental measurements for case HP-fb.

The graph highlights that penetration length is overestimated using only the aerodynamic breakup model. This result has been already observed by the authors studying the Spray G with the same approach [23].

Figure 11 depicts the spray morphology at 0.4375 ms after the SOI; the droplets are represented, and they are colored accordingly with their diameter.

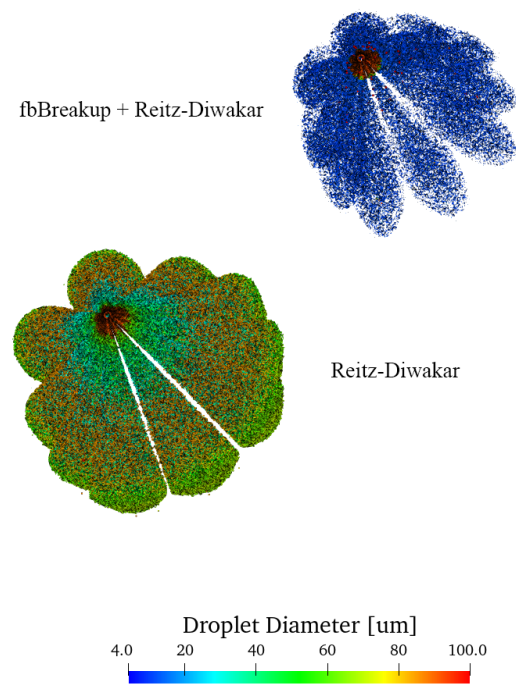


Figure 11. Spray morphology represented coloring liquid droplets accordingly with their diameter. $t = 0.4375$ ms after the SOI. Case HP-fb simulated using fbBreakup+Reitz–Diwakar model is reported on top while simulation with only the Reitz–Diwakar model on bottom.

The effervescent breakup model predicts droplets approximately one order of magnitude smaller than what computed using only the **Reitz–Diwakar** model. Figure 12 shows the droplet size distributions obtained with **fbBreakup+Reitz–Diwakar** model and with only the **Reitz–Diwakar** model.

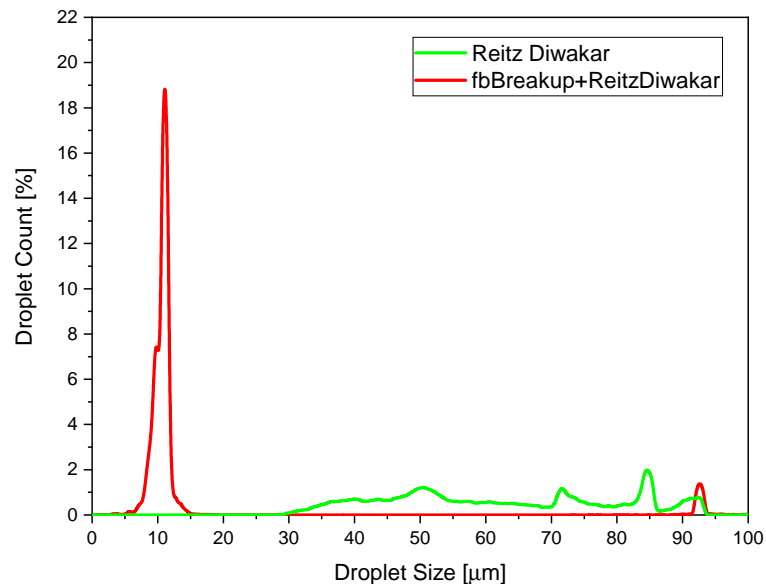


Figure 12. Predicted droplet size distributions for case HP-fb at 0.4 ms after SOI.

The parcels obtained from the **fbBreakup+Reitz–Diwakar** model have an average value equal to approximately 10 μm while using the **Reitz–Diwakar** model parcel’s diameter ranges between 40 μm –80 μm without a pseudo-average value. The different droplet size distribution influences also fuel vaporization. Figure 13 reports the vapor fuel mass in the computational domain as a function of the time elapsed from the start of the injection event.

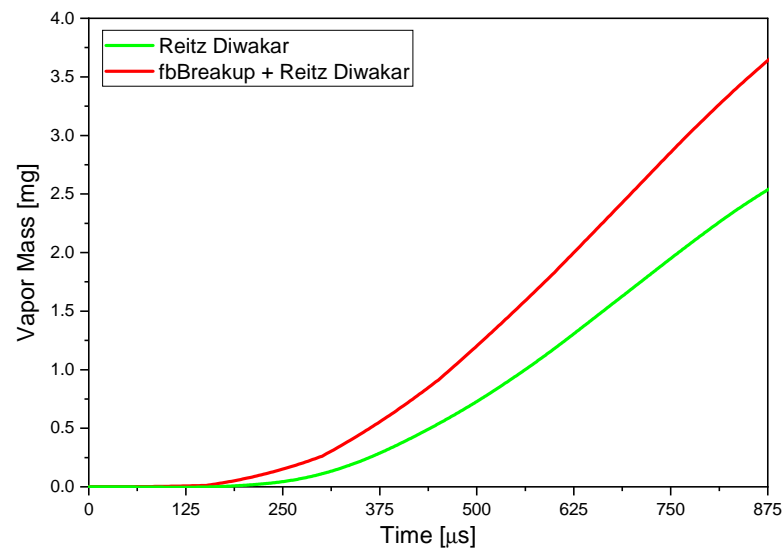


Figure 13. Vaporized fuel mass as function of elapsed time from the beginning of the injection.

The **fbBreakup** model promotes fuel vaporization indeed, after 750 μs, the fuel evaporated is 20% greater.

3.3. Details about the Spray Morphology

After assessing the accuracy of CFD results with experiments, as well as the role of the effervescent breakup model, the simulation results were used to shed more light on other spray characteristics. Figure 14 is a snapshot taken at 0.4375 ms after the where spray’s droplets are represented and colored proportionately to their diameter for case vHP (top) and for case vHP-fb (bottom).

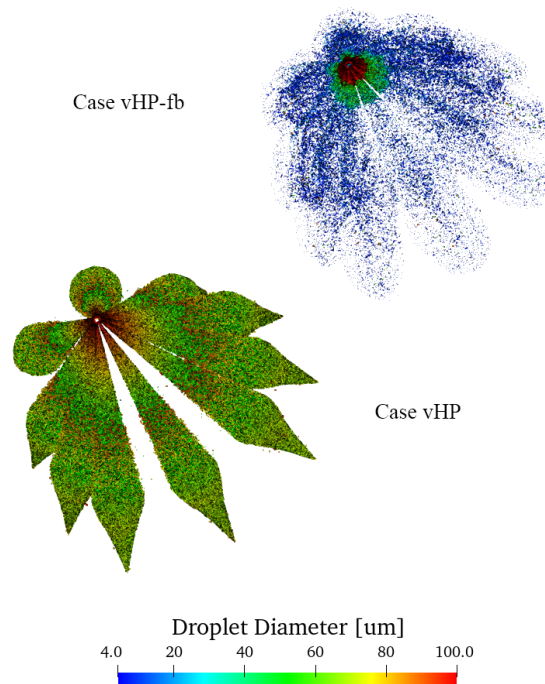


Figure 14. Spray morphology for the cases vHP-fb (top) and vHP (bottom) represented with droplets colored accordingly with their diameter at 0.4375 ms after the SOI.

Flash boiling promotes both breakup and evaporation radically changing the morphology of the spray. The plumes of the flashing spray exhibit the interaction typical of a

flash-boiling spray and are composed by smaller droplets. Figure 15 shows a volumetric rendering of the fuel mass fraction ($Y_{IC_8H_{18}}$) evaporated after 0.4375 ms from the SOI for case vHP.

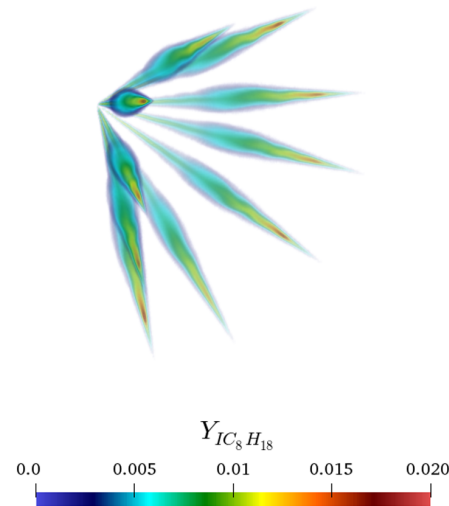


Figure 15. 3D visualization of the concentration of the vaporized fuel.

The amount of fuel vaporized is negligible because the injection takes place in non-evaporative conditions. More interesting is the case vHP-fb. Figure 16 reports the temporal evolution of the evaporated fuel for case vHP-fb.

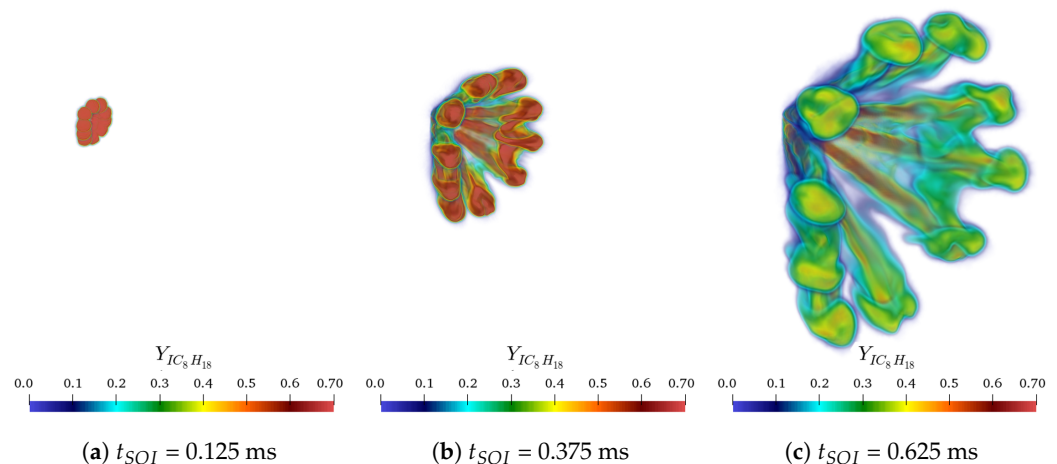


Figure 16. 3D visualization of the concentration of the vaporized fuel.

The vaporization process regards only the core of the single plumes because the ambient temperature is lower (only 293 K) than the fuel one. The images indicate a not-severe plume-to-plume interaction but intense enough to entail great compactness of the spray, also in terms of vaporized fuel. Figure 17 shows the droplet's Sauter mean Diameter (SMD_{32}) as a function of the axial distance for case vHP and case vHP-fb.

The effervescent breakup strongly influences the morphology of the spray issued in the flash boiling condition. At a distance between 5 and 10 mm, the effervescent breakup reduces of approximately one order of magnitude the droplet's dimension. The decrease of the SMD is much slighter in non-evaporative conditions. This is expected because the aerodynamic breakup is weaker if compared to the thermodynamic breakup mechanism.

Figure 18 shows the droplet's Sauter mean Diameter (SMD_{32}) vs the axial distance for the two injection pressures tested in flashing conditions.

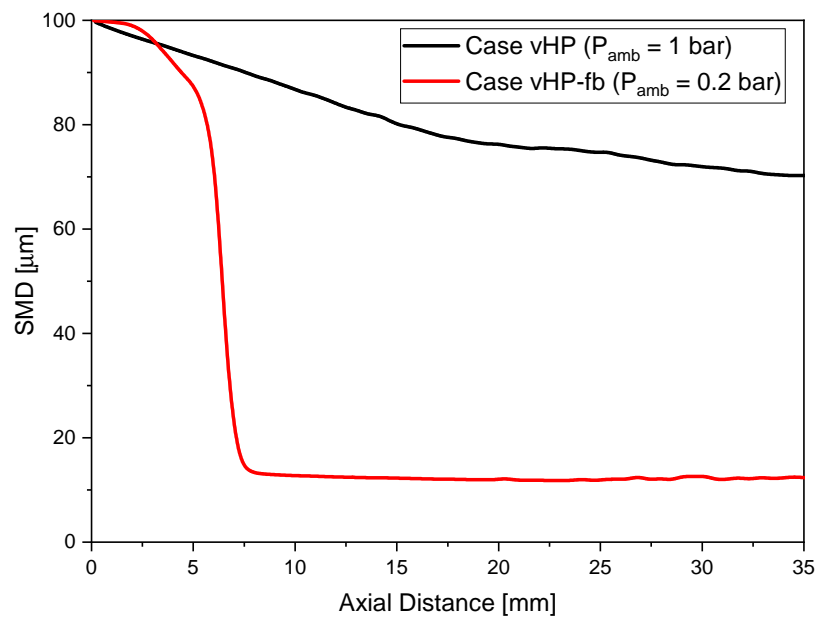


Figure 17. Average SMD as a function of the axial distance from injector tip for cases vHP and case vHP-fb.

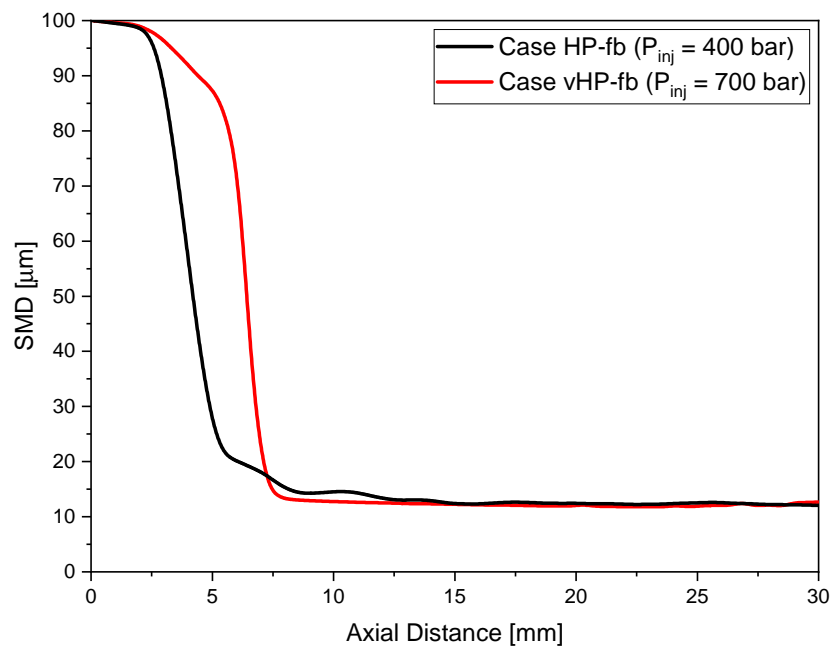


Figure 18. Average SMD as a function of the axial distance from injector tip for cases vHP and case vHP-fb.

The higher the injection pressure, the more downstream flash boiling breakup happens. This is a consequence of the higher injection pressure which gives to the jet an higher momentum leading to an extension of the flash-boiling breakup length. Furthermore, the higher injection pressure has two positive effects on the spray morphology. Figure 19 reports the droplet’s size distribution for the two injection pressures investigated.

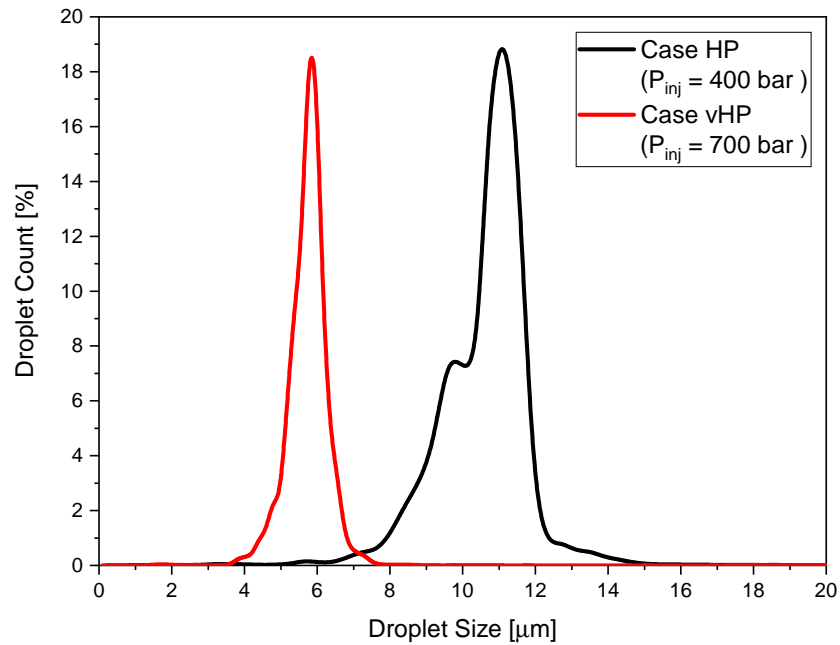


Figure 19. Predicted droplet size distributions for case HP and vHP at 0.43 ms after SOI.

An increase in such a parameter brings in having a more atomized spray, as demonstrated by the plot where the mean value of the distribution decrease as the injection pressure increases. The high injection pressure permits also to avoid an important undesired effect of flash-boiling: the spray collapse. Figure 20 is a representation of the spray where the interaction between air and fuel was highlighted over-imposing the velocity vectors on the vaporized fuel mass fraction. Case HP-fb is reported on the left and case HP-fb is reported on the right.

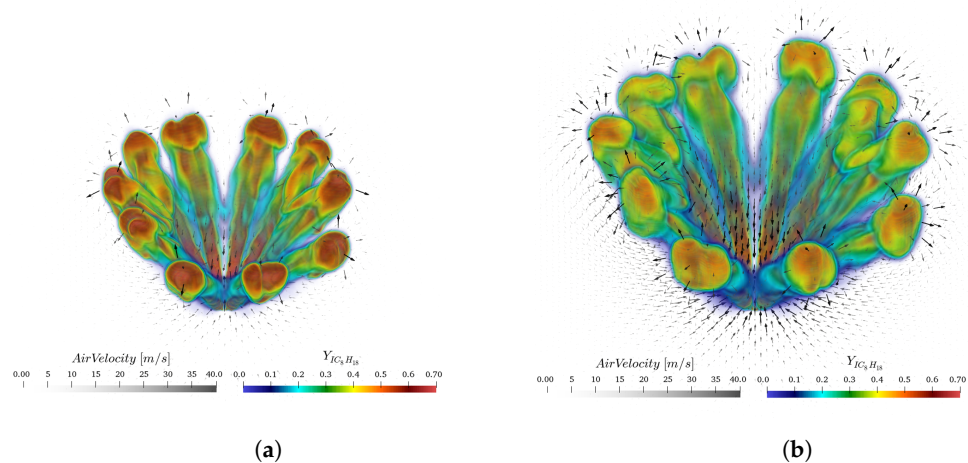


Figure 20. Velocity vectors and vapor mass fraction at $t_{SOI} = 0.43$ ms for cases HP-fb (a) and vHPfb (b).

The velocity vectors demonstrate how the air flows from the bottom of the spray toward the injector’s nozzle avoiding the pressure reduction in the central region of the spray and promoting the mixture formation. This flow pattern inhibits also the spray collapse, which is one of the major causes of spray-wall impingement.

Further than improving spray breakup and vaporization, flash-boiling promotes also the turbulence generation and, consequently, air-fuel mixing [8]. Here, to evaluate the self-generated turbulence, vortices were represented as Q-criterion isosurfaces and colored accordingly with total turbulent kinetic energy (TKE). Figure 21 reports such elaboration for cases vHP and vHP-fb.

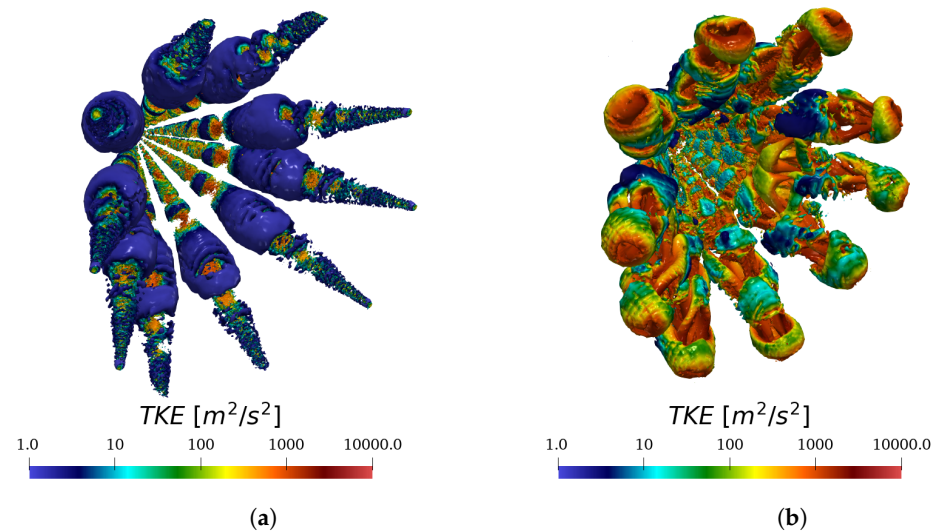


Figure 21. Q-criterion isosurfaces colored by total TKE for case vHP (a) and vHP-fb (b).

The vortices spin around the axis of the single plume; their development is critical for air entrainment in the plume's core to support the mixture formation. It is important to highlight also how moving from non-evaporative to flash-boiling conditions, the vortices dimension as well as TKE (turbulent kinetic energy) severally increase.

4. Conclusions

The analysis of the injection process in flash boiling conditions of a spray issued from an innovative multi-hole operating at of ultrahigh injection pressure was carried out. Experimental images of the spray acquired using shadowgraph technique were exploited to validate Eulerian–Lagrangian simulations of nonevaporative and flash-boiling conditions. The flash-boiling conditions considered were simulated using an effervescent breakup model, based on vapor bubbles growing within the liquid droplets, together with Reitz–Diwakar aerodynamic breakup model.

The main outcomes can be summarized as follows:

- Subcooled and flash-boiling sprays can be reproduced with no changes the breakup constants by using an effervescent breakup model when superheated conditions are simulated.
- Compared to an aerodynamic breakup model alone, the effervescent breakup model predicts droplets with smaller dimensions. The size distribution resemble a Gaussian distribution while, using Reitz–Diwakar model, the droplets' diameters range from $40\ \mu\text{m}$ to $80\ \mu\text{m}$.
- The Reitz–Diwakar breakup model alone overestimates spray penetration when the constants used for nonevaporative conditions are used for flash-boiling conditions.
- The effervescent breakup reduces the droplet diameter of about one order of magnitude (catastrophic breakup) at a distance which, depending on the injection pressure, ranges between 5 and 10 mm from the injector tip.
- For the investigated cases, plume-to-plume interaction is significantly promoted by flash-boiling occurrence, but it is not strong enough to cause spray collapse.
- Adopting an elevated values of injection pressures spray-collapse is avoided, and so air/fuel interaction is promoted as well as ambient gas recirculation.
- Switching from nonevaporative to flash-boiling conditions both the turbulent kinetic energy and the dimensions of the vortical structures increase.

Future works will regard coupling of Eulerian near-nozzle and Eulerian–Lagrangian simulations to initialize the spray simulation properly and the investigation of even higher injection pressures.

Author Contributions: F.D.: Conceptualisation, methodology, software, data curation, validation, visualization, writing—original draft. A.D.V.: Writing—review and editing, supervision, project administration. A.M.: Investigation, resources, writing—review and editing. L.A.: Investigation, resources, writing—review and editing. All authors have read and agreed to the published version of the manuscript.

Funding: This research received no funding.

Institutional Review Board Statement: Not applicable.

Informed Consent Statement: Not applicable.

Data Availability Statement:

Acknowledgments: All the simulations were performed with the developed solver on the Galileo100 cluster of HPC CINECA facilities within the agreement between DIIE—Università degli Studi dell’Aquila and CINECA.

Conflicts of Interest: The authors declare no conflict of interest.

Abbreviations

The following abbreviations are used in this manuscript:

<i>AMR</i>	Adaptive Mesh Refinement
<i>CFD</i>	Computational Fluid Dynamic
<i>DDM</i>	Discrete Droplet Model
<i>ECN</i>	Engine Combustion Network
<i>GDI</i>	Gasoline Direct Injection
<i>HRM</i>	Homogeneous Relaxation Model
k_b	Breakup criterion
k_v	Constant for spray expansion
$KH - RT$	Kelvin–Helmholtz–Rayleigh–Taylor
Ma_i	Bubble Mach number
n	Number of particles
P_∞	Ambient pressure
p_{amb}	Nominal ambient pressure
P_{sat}	Liquid saturation pressure
<i>PISO</i>	Pressure Implicit with splitting of operator
<i>PIV</i>	Particle Image Velocimetry
$R_{i,0}$	Initial vapor bubble radius
R_0	Droplet radius
R_i	Vapor bubble radius
R_p	Ambient to saturation pressure ratio
<i>RANS</i>	Reynolds-Averaged Navier–Stokes
<i>RD</i>	Reitz–Diwakar
SMD_{32}	Sauter Mean Diameter
SMR_{32}	Sauter Mean Radius
<i>SOI</i>	Start Of Injection
<i>SVCO</i>	Stepped Hole Valve Covered Orifice
T_{sat}	Saturation temperature
T_0	Liquid temperature
t_b	Bubble breakup time
U_r	Magnitude of radial velocity
V_i	Bubble grow rate
V_o	Droplet grow rate
<i>VOF</i>	Volume Of Fluid
We_i	Bubble Weber number
We_o	Droplet Weber number
η	Disturbance
η_0	Initial disturbance
μ	Dynamic viscosity

ω	Instability grow rate
ψ_o	Air–Liquid density ratio
ψ_i	Bubble–Liquid density ratio
ρ_{gi}	Inner gas density
ρ_{go}	Outer gas density
ρ_l	Liquid density
σ	Liquid surface tension

References

1. Payri, R.; Salvador, F.J.; Martí-Aldaraví, P.; Vaquerizo, D. ECN Spray G external spray visualization and spray collapse description through penetration and morphology analysis. *Appl. Therm. Eng.* **2017**, *112*, 304–316. [\[CrossRef\]](#)
2. Di Ilio, G.; Krastev, V.K.; Falcucci, G. Evaluation of a Scale-Resolving Methodology for the Multidimensional Simulation of GDI Sprays. *Energies* **2019**, *12*, 2699. [\[CrossRef\]](#)
3. Duronio, F.; De Vita, A.; Allocca, L.; Anatone, M. Gasoline direct injection engines—A review of latest technologies and trends. Part 1: Spray breakup process. *Fuel* **2020**, *265*, 116948. [\[CrossRef\]](#)
4. Nocivelli, L.; Sforzo, B.A.; Tekawade, A.; Yan, J.; Powell, C.F.; Chang, W.; Lee, C.F.; Som, S. *Analysis of the Spray Numerical Injection Modeling for Gasoline Applications*; SAE Technical Papers; SAE International: Warrendale, PA, USA, 2020.
5. Zembi, J.; Mariani, F.; Battistoni, M.; Irimescu, A.; Merola, S. *Numerical Investigation of Water Injection Effects on Flame Wrinkling and Combustion Development in a GDI Spark Ignition Optical Engine*; SAE WCX Digital Summit; SAE International: Warrendale, PA, USA, 2021.
6. Oh, H.; Hwang, J.; Pickett, L.M.; Han, D. Machine-learning based prediction of injection rate and solenoid voltage characteristics in GDI injectors. *Fuel* **2022**, *311*, 122569. [\[CrossRef\]](#)
7. Duronio, F.; De Vita, A.; Montanaro, A.; Villante, C. Gasoline direct injection engines—A review of latest technologies and trends. Part 2. *Fuel* **2020**, *265*, 116947. [\[CrossRef\]](#)
8. Youso, T.; Fujikawa, T.; Yamakawa, M.; Kaminaga, T.; Yamaguchi, K.; Ratnak, S.; Kusaka, J. A Study on Combustion Characteristics of a High Compression Ratio SI Engine with High Pressure Gasoline Injection. In Proceedings of the 14th International Conference on Engines & Vehicles, Beijing, China, 28 July–1 August 2019; SAE International: Warrendale, PA, USA, 2019.
9. Karrholm, F.P.; Helmantel, A.; Koopmans, L.; Dahlander, P.; Yamaguchi, A. Spray Characterization of Gasoline Direct Injection Sprays Under Fuel Injection Pressures up to 150 MPa with Different Nozzle Geometries. In Proceedings of the International Powertrains, Fuels & Lubricants Meeting, Kyoto, Japan, 26–29 August 2019; SAE International: Warrendale, PA, USA, 2019.
10. Fatouraie, M.; Medina, M.; Wooldridge, M. High-Speed Imaging Studies of Gasoline Fuel Sprays at Fuel Injection Pressures from 300 to 1500 bar. In Proceedings of the WCX World Congress Experience, Detroit, MI, USA, 10–12 April 2018; SAE International: Warrendale, PA, USA, 2018.
11. Guo, H.; Li, Y.; Lu, X.; Zhou, Z.; Xu, H.; Wang, Z. Radial expansion of flash boiling jet and its relationship with spray collapse in gasoline direct injection engine. *Appl. Therm. Eng.* **2019**, *146*, 515–525. [\[CrossRef\]](#)
12. Xu, M.; Zhang, Y.; Zeng, W.; Zhang, G.; Zhang, M. Flash Boiling: Easy and Better Way to Generate Ideal Sprays than the High Injection Pressure. *SAE Int. J. Fuels Lubr.* **2013**, *6*, 137–148. [\[CrossRef\]](#)
13. Sher, E.; Bar-Kohany, T.; Rashkovan, A. Flash-boiling atomization. *Prog. Energy Combust. Sci.* **2008**, *34*, 417–439. [\[CrossRef\]](#)
14. Bar-Kohany, T.; Sher, E. Flash boiling atomization under negative pressure conditions. *At. Sprays* **2021**, *31*, 1–8. [\[CrossRef\]](#)
15. Lefebvre, A.H.; McDonell, V.G. *Atomization and Sprays*; CRC Press: Boca Raton, FL, USA, 2017.
16. Brennen, E. *Cavitation and Bubble Dynamics* Christopher; California Institute of Technology Pasadena: Pasadena, CA, USA, 1995.
17. Wang, B.; Mosbach, S.; Schmutzhard, S.; Shuai, S.; Huang, Y.; Kraft, M. Modelling soot formation from wall films in a gasoline direct injection engine using a detailed population balance model. *Appl. Energy* **2016**, *163*, 154–166. [\[CrossRef\]](#)
18. Zeng, W.; Xu, M.; Zhang, G.; Zhang, Y.; Cleary, D.J. Atomization and vaporization for flash-boiling multi-hole sprays with alcohol fuels. *Fuel* **2012**, *95*, 287–297. [\[CrossRef\]](#)
19. Chan, Q.N.; Bao, Y.; Kook, S. Effects of injection pressure on the structural transformation of flash-boiling sprays of gasoline and ethanol in a spark-ignition direct-injection (SID) engine. *Fuel* **2014**, *130*, 228–240. [\[CrossRef\]](#)
20. Allocca, L.; Montanaro, A.; Meccariello, G. Effects of the Ambient Conditions on the Spray Structure and Evaporation of the ECN Spray G. In Proceedings of the WCX SAE World Congress Experience, Detroit, MI, USA, 9–11 April 2019; SAE International: Warrendale, PA, USA, 2019.
21. Migliaccio, M.; Montanaro, A.; Paredi, D.; Lucchini, T.; Allocca, L.; D’Errico, G. *CFD Modeling and Validation of the ECN Spray G Experiment under a Wide Range of Operating Conditions*; SAE Technical Papers; SAE International: Warrendale, PA, USA, 2019.
22. Duronio, F.; De Vita, A.; Allocca, L.; Montanaro, A.; Ranieri, S.; Villante, C. *CFD Numerical Reconstruction of the Flash Boiling Gasoline Spray Morphology*; SAE Technical Papers; SAE International: Warrendale, PA, USA, 2020.
23. Duronio, F.; Mascio, A.D.; Villante, C.; Anatone, M.; Vita, A.D. ECN Spray G: Coupled Eulerian internal nozzle flow and Lagrangian spray simulation in flash boiling conditions. *Int. J. Engine Res.* **2023**, *24*, 14680874221090732. [\[CrossRef\]](#)
24. Duronio, F.; Montanaro, A.; Ranieri, S.; Allocca, L.; De Vita, A. Under-Expanded Jets Characterization by Means of CFD Numerical Simulation Using an Open FOAM Density-Based Solver. In Proceedings of the 15th International Conference on Engines & Vehicles, Napoli, Italy, 12–16 September 2021; SAE International: Warrendale, PA, USA, 2021.

25. Montanaro, A.; Allocca, L.; Ranieri, S.; Beatrice, C. Computational-Experimental Framework for Realizing a Novel Apparatus for Supercritical Water by Induction Heating. *Heat Transf. Eng.* **2022**, *44*, 785–802. [[CrossRef](#)]
26. Duronio, F.; Montanaro, A.; Allocca, L.; Ranieri, S.; De Vita, A. Effects of Thermodynamic Conditions and Nozzle Geometry on the Methane Direct Injection Process in Internal Combustion Engines. In Proceedings of the WCX SAE World Congress Experience, Detroit, MI, USA, 5–7 April 2022; SAE International: Warrendale, PA, USA, 2022.
27. Stiesch, G. *Modeling Engine Spray and Combustion Processes*; Springer Science & Business Media: Berlin/Heidelberg, Germany, 2003.
28. Duronio, F.; Ranieri, S.; Montanaro, A.; Allocca, L.; De Vita, A. ECN Spray G injector: Numerical modelling of flash-boiling breakup and spray collapse. *Int. J. Multiph. Flow* **2021**, *145*, 103817. [[CrossRef](#)]
29. Zeng, Y. Modelling of Multicomponent Fuel Vaporization in Internal Combustion Engines. Ph.D. Thesis, University of Illinois at Urbana-Champaign, Champaign, IL, USA, 2000.
30. Richards, K.; Senecal, P.; Pomraning, E. *Converge 3.0*; Convergent Science: Madison, WI, USA, 2021.
31. Price, C.; Hamzehloo, A.; Aleiferis, P.; Richardson, D. Numerical modelling of fuel spray formation and collapse from multi-hole injectors under flash-boiling conditions. *Fuel* **2018**, *22*, 518–541. [[CrossRef](#)]
32. Paredi, D.; Lucchini, T.; D’Errico, G.; Onorati, A.; Pickett, L.; Lacey, J. Validation of a comprehensive computational fluid dynamics methodology to predict the direct injection process of gasoline sprays using Spray G experimental data. *Int. J. Engine Res.* **2020**. [[CrossRef](#)]
33. Bilicki, Z.; Kestin, J.; Stuart, J.T. Physical aspects of the relaxation model in two-phase flow. *Proc. R. Soc. Lond. Math. Phys. Sci.* **1990**, *428*, 379–397.
34. Reitz, R. Modeling atomization processes in high-pressure vaporizing sprays. *At. Spray Technol.* **1987**, *3*, 309–337.
35. Faeth, G. Current status of droplet and liquid combustion. *Prog. Energy Combust. Sci.* **1977**, *3*, 191–224. [[CrossRef](#)]
36. Amsden, A.A.; O’Rourke, P.J.; Butler, T.D. *KIVA-II: A Computer Program for Chemically Reactive Flows with Sprays*; Los Alamos National Lab.: Los Alamos, NM, USA, 1989.
37. Price, C.; Hamzehloo, A.; Aleiferis, P.; Richardson, D. An approach to modeling flash-boiling fuel sprays for direct-injection spark-ignition engines. *At. Sprays* **2016**, *26*, 1197–1239. [[CrossRef](#)]
38. Senecal, P.K.; Pomraning, E.; Richards, K.J.; Som, S. Grid-Convergent Spray Models for Internal Combustion Engine Computational Fluid Dynamics Simulations. *J. Energy Resour. Technol.* **2013**, *136*, 012204. [[CrossRef](#)]
39. Di Angelo, L.; Duronio, F.; De Vita, A.; Di Mascio, A. Cartesian Mesh Generation with Local Refinement for Immersed Boundary Approaches. *J. Mar. Sci. Eng.* **2021**, *9*, 572. [[CrossRef](#)]
40. Roache, P.J. Quantification of uncertainty in computational fluid dynamics. *Annu. Rev. Fluid Mech.* **1997**, *29*, 123–160. [[CrossRef](#)]

Disclaimer/Publisher’s Note: The statements, opinions and data contained in all publications are solely those of the individual author(s) and contributor(s) and not of MDPI and/or the editor(s). MDPI and/or the editor(s) disclaim responsibility for any injury to people or property resulting from any ideas, methods, instructions or products referred to in the content.